# Consideration of temperature monitoring channel number for divertor heat flux profile reconstruction in commercial fusion reactors

XNS. Bui,[1] H. Matsuura,[2] Y. Hayashi,[3,4] K. Nagaoka,[3,5] and S. Masuzaki[3,4]
[1)]*Osaka Prefecture University, Osaka 599-8570, Japan*
[2)]*Osaka Metropolitan University, Osaka 599-8570, Japan*
[3)]*National Institute for Fusion Science, Toki 509-5292, Japan*
[4)]*The Graduate University for Advanced Studies, SOKENDAI, Toki 509-5292, Japan*
[5)]*Nagoya University, Nagoya 464-8601, Japan*

(*The author to whom correspondence may be addressed:XNS. BUI mc106010@st.osakafu-u.ac.jp)

(Dated: 3 August 2023)

In the fusion demonstration (DEMO) reactors, to keep Tritium breeding rate TBR>1 and adapt the first wall and divertor requirement related to high heat load and neutron shielding, the number of port plugs and other openings must be limited. In such a scenario, developing alternative methods instead of using infra-red (IR) thermography to determine peak heat flux and heat flux profile onto divertor target is necessary. The divertor tile equipped with thermocouples (TCs) can be one of the candidates for heat flux monitoring in DEMO reactors. Multiple temperature monitoring channels can be set as an array along the observed tile to reproduce the temperature profile. In DEMO, to avoid the high temperature as well as high neutron flux environment, the monitoring positions can be set further from the irradiation surface. However, the spatial resolution of this method is lower in comparison to that of the IR cameras. We apply 2D temperature response functions and the corresponding heat conduction model to LHD divertor tile surface temperature data to study the effect of monitored temperature profile spatial resolution to the reconstructed heat flux profile. This might provide some helpful information to define the method of embedding TCs to the divertor tiles in future DEMO reactors.

## I. INTRODUCTION

In the operation of magnetically confined fusion devices, plasma heat fluxes induce temperature increments in divertor plates and other plasma facing components (PFCs). The plasma heat flux in ITER is expected to be in the order of 10 $\mathrm{MWm}^{-2}$ during steady state and even much higher at transition phases.[1] Such heat fluxes must be handled to prevent PFCs damage owing to material erosion. Thus, developing methods for heat flux measurements is necessary. The accuracy of heat flux measurement depends on temperature evolution data and heat conduction model. In detail, the evaluated heat flux is only valid when it can reproduce the monitored temperature evolution with the heat conduction model.

Currently, Infrared (IR) thermography is a popular and reliable method to monitor temperature and heat flux into divertor targets.[2–5] In the fusion demonstration (DEMO) reactors, however, divertor heat flux estimation becomes more challenging. To keep Tritium breeding rate TBR>1 and adapt the first wall and divertor requirement related to high heat load and neutron shielding, the number of port plugs and other openings must be limited.[6–8] In such a scenario, measurements with IR cameras can be unavailable. Other types of thermometers such as Langmuir probes[9,10], optical fiber[11,12], or thermocouples (TCs)[13–17] have been applied for divertor heat flux analysis. For DEMO, the divertor tile equipped with thermocouples (TCs) can be a good candidate because it does not require any opening area for temperature monitoring and its time resolution in the order of ms can provide the detailed temperature time evolution. However, the limited spatial resolution of this method causes difficulty to reconstruct heat flux spatial profiles with numerical methods.

Inverse heat flux evaluation from temperature data can be obtained with a heat conduction model. Such a model assumes the control volume (CV) containing the temperature measurement point, and must satisfy energy conservation law. Heat flux crossing the boundary, heat generation in the CV, and internal energy evolution must be balanced. Temperature response in the CV can be described as a 1-dimensional (1D) function and it varies with different conditions at the backside boundary.[15] By interactive fitting such a function to temperature data the heat flux time evolution can be analytically deduced while keeping the target's heat balance.[16,17]

In this work, we expanded the temperature response function to 2-dimension (2D) to analyze the temperature data of a divertor tile obtained by IR thermography in the Large Helical Device (LHD).[4] This method provides temperature and heat flux spatial profiles, as well as their time evolution. Moreover, the response function is applied to different down-sampled temperature patterns to study the effect of spatial resolution on the reconstructed heat flux profiles. This might be helpful to determine TCs embedding methods in DEMO's divertor targets In the next section, 1D temperature response function is introduced. In section III, an analysis of temperature data in LHD divertor tile using 2D temperature response function is presented. Section IV is discussion and conclusion.

## II. 1D TEMPERATURE RESPONSE FUNCTION

Figure 1 shows the schematic of a sensor target where $L_x$ and $L_z$ are its width and thickness, respectively. The target is considered as a CV containing the temperature measurement point. The 1D temperature response function is determined by assuming that the boundary at $z = 0$ is irradiated by a homogeneous heat flux. To ensure heat balance in the CV, the

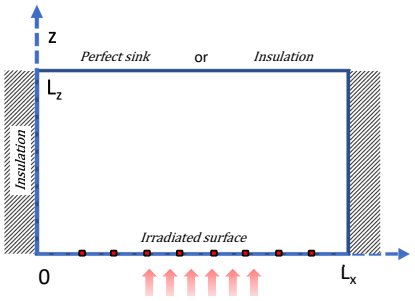


FIG. 1. A rectangular target is modeled for defining temperature response function

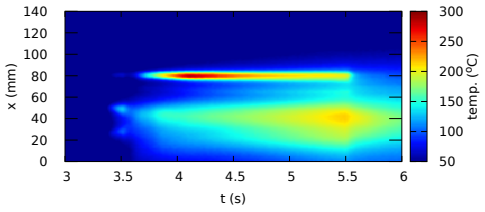


FIG. 2. Time evolution of a temperature profile obtained by IR camera (discharge number 151745)

response function must satisfy 1D heat conduction equation. In general, this balance depends on the cooling system of the target and choices of back-side boundary condition at $z = L_z$.

Temperature response functions $S(z,t)$ of step-like heat flux with different back-side boundary conditions has been proposed[15] and successfully explained the effect of TC signal time delay owing to the target thermal diffusion time. By fitting the response function to measured temperature data, the time-dependent heat flux can be estimated. This method, so-called pulse decomposition, has been applied to analyse the divertor heat flux in LHD[16] and GAMMA 10/PDX[17]. The estimated heat flux is averaged for the whole target area which might be relevant for small sensor targets.

Figure 2 indicates the surface temperature profile and its time evolution at $z = 0$ obtained by an IR thermography system in LHD divertor tile[4]. This data set corresponds to the discharge shot number 151745, where the plasma started at ∼3.5 s and stopped at ∼5.5 s. The temperature data obviously shows two temperature peaks at x= 40 mm and x = 80 mm. The tile of consideration consists of a graphite layer with $L_z = 15$ mm. A heat sink system is embedded behind the tile for heat removal.

Equation (3) in[15] describes a temperature response function assuming that the temperature at $z = L_z$ is kept at background temperature by a heat sink. Such a response function is incorporated with the pulse decomposition method[16] to estimate heat flux evolutions from the temperature data extracted from figure 2. The heat flux evolutions estimated from the temperature data at $x = 40$mm and $x = 80$mm are shown in figure 3. Note that the heat flux evolution is averaged for $0 < x < L_x$. The monitored temperature evolutions and that reproduced by

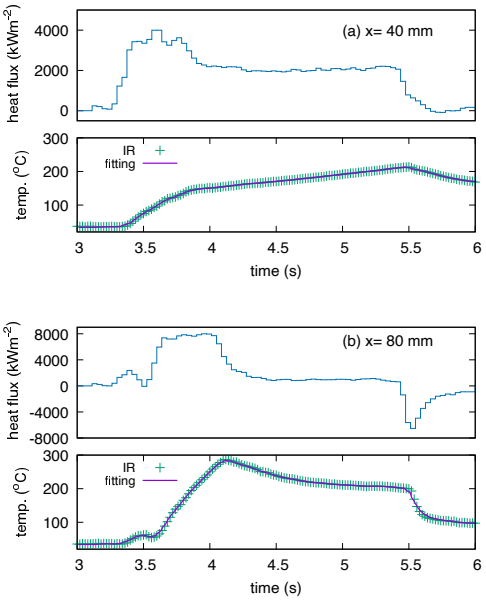


FIG. 3. Heat flux evolutions estimated by pulse decomposition method[16] and $S(z,t)$ function at (a) x= 40 mm, and (b) x=80 mm.

1D temperature response function are indicated by the green scatters and the magenta solid line, respectively. Owing to the profile effect, the temperature evolution at $x = 40$mm [see figure 3 (a)] is much different from that at $x = 80$mm [see figure 3 (b)]. This induces the differences corresponding to tendency and peak value in the heat flux evolutions. Besides, severe negative heat flux value can be found in figure 3 (b) at $t = 5.5s$ when the heating pulse terminated. With the 1D temperature response function $S(z,t)$, the heat flux at z=0 must be small to reproduce temperature decrements. If the temperature drastically decreases, results with negative heat fluxes are inevitable. However, this unreasonable point can be overcome by consideration of heat diffusion in the other spatial directions.

## III. 2D TEMPERATURE RESPONSE FUNCTION

With the consideration of profile effect in divertor tiles, expanding the response function to $x$ direction is necessary. In this approach, the response functions become 2-dimensional including parallel and perpendicular directions to the tile surface. To determined 2D temperature response function, the target indicated in figure 1 is assumed to be irradiated by the step-like heat flux with normalized profile $f(x)$ in the front boundary $z = 0$.

$$q(t) = \begin{cases} 0 & (t < 0) \\ q_0 f(x) & (t > 0) \end{cases} \tag{1}$$

Side boundaries at $x = 0$ and $x = L_x$ are assumed to be thermal insulated $\frac{\partial T}{\partial x} = 0$. Background temperature when $t < 0$ is denoted by $T_0$. The response function $S(x,z,t)$=$T(x,z,t) - T_0$

for this step-like heat flux in asymptotic solution can be generalized as

$$S(x,z,t) = \begin{cases} 0 & (t<0) \\ \Delta T\left(\frac{1}{2}\alpha_0 g_0\left(\frac{z}{L_z}\right) + \sum_{n=0}^{n_{max}} \alpha_n g_n\left(\frac{z}{L_z}\right)\cos\left(n\pi\frac{x}{L_x}\right)\right) & (t>0) \end{cases} \tag{2}$$

where $\Delta T = \frac{q_0 L_z}{\kappa}$. Equation $g_0$ and $g_n$ depend on back-side boundary condition. Coefficients $\alpha_0$ and $\alpha_n$ are defined by expanding the heat flux profile $f(x)$ as

$$f(x) = \frac{1}{2}f_0 + \sum_{n=0}^{n_{max}} f_n \cos\left(B_n \frac{x}{L_x}\right) \tag{3}$$

where $B_n = n\pi$.

In this work, the temperature response functions are defined for two different conditions in the back-side boundary. One assume that the temperature in the back-side boundary is kept to be $T_0$ by a perfect heat sink so that the target temperature does not increase during the discharge. Another assumes that the back-side boundary is thermally insulated $\frac{\partial T}{\partial x} = 0$. Function $g_0$ is referenced from the asymptotic term of the temperature response functions in[15]. In the insulation case, function $g_0$ contains a time-dependent term where the time variable $t$ is normalized with $\tau$. $\tau = \frac{4}{\pi^2}\frac{L_z^2}{\alpha}$ deduced from 2D heat conduction equation $\frac{1}{\alpha}\frac{\partial T}{\partial t} = \frac{\partial^2 T}{\partial x^2} + \frac{\partial^2 T}{\partial z^2}$, $\left(\frac{C_n}{L_z}\right)^2 = \left(\frac{B_n}{L_x}\right)^2$ where $\kappa$ and $\alpha = \frac{\kappa}{c\rho}$ are heat conductivity and thermal diffusivity of the divertor tile material.

Table I summaries the dependence of the temperature response function on back-side boundary conditions. The back-side boundary conditions lead to different temperature profiles even with the same heat flux profile applied to the front boundary at $z = 0$.

TABLE I. Dependence of coefficients on back-side boundary conditions

| | Prefect sink | Insulation |
|---|---|---|
| $g_0$ | $1-\frac{z}{L_z}$ | $\frac{4}{\pi^2}\frac{t}{\tau} - \frac{z}{L_z} + \frac{1}{2}(\frac{z}{L_z})^2$ |
| $g_n$ | $\sinh(C_n(1-\frac{z}{L_z}))$ | $\cosh(C_n(1-\frac{z}{L_z}))$ |
| $\alpha_0$ | $f_0$ | $f_0$ |
| $\alpha_n$ | $\frac{f_n}{C_n\cosh(C_n)}$ | $\frac{f_n}{C_n\sinh(C_n)}$ |

Effects of back-side boundary conditions are illustrated in figure 4. Here the target is assumed to be graphite with $L_z = 15$ mm and $L_x = 143$mm. The heat flux with $q_0 = 1$ MWm$^{-2}$ and normalized profile $f(x)$ is illustrated in figure 4 (a). The temperature profile in the target can be obtained by equation (2). Figure 4 (b) and 4 (c) indicate the temperature profiles with insulation and sink back-side boundary, respectively. In figure 4 (b), the heat accumulation can be observed at the back-side as no heat transfer occur. In the heat sink case, the temperature profile in figure 4 (c) has lower peak values with no temperature increment at $z = 143$ mm.

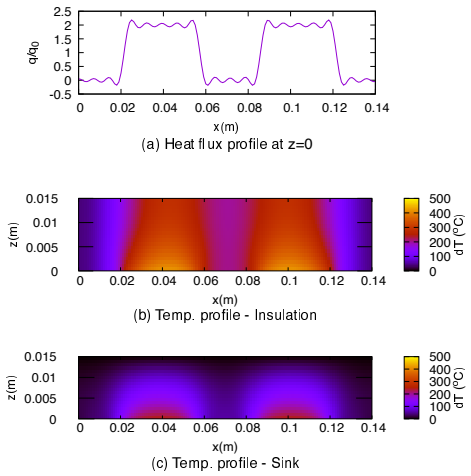


FIG. 4. From (a) the same heat flux profile at z = 0, the temperature profiles determined with (b) insulation-, and (c) sink back-side boundaries are very different.

Before applying the temperature response function to analysis, carefully determining the back-side boundary condition is important. The perfect sink and perfect insulation boundary conditions, however, are not realistic. The heat sink boundary condition is not reasonable for long-time irradiation. Besides, it is difficult to ensure that there is no heat exchange occurring in the thermal insulation boundary. In the real experiments, the back-side boundary condition is somewhere between the two cases provided in this work.

### A. Reconstruction of temperature and heat flux profile

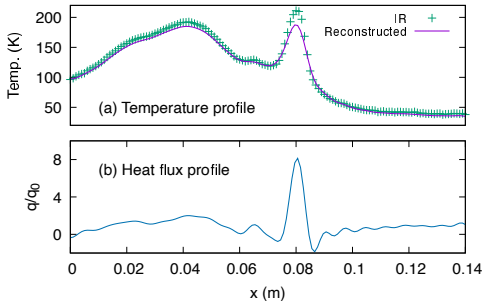


FIG. 5. (a) Fitting function $S(x,z,t)$ to IR data makes it possible to obtain the (b) heat flux profile at t = 5s.

As heat removal is processed by the heat sink system behind the LHD divertor tiles, equation (2) with heat sink backside boundary condition is chosen to analyze the temperature profiles in figure 2. Here the response function is defined with $L_x = 143$mm, $L_z = 15$mm, and the thermal properties of isotropic graphite. Coefficients $\alpha_0$ and $\alpha_n$ for the temperature profile can be obtained by interactively fitting the response function to the temperature data along $x$ direction. After that, coefficient $f_n$ for the heat flux profile can be estimated from $\alpha_0$ and $\alpha_n$.

Figure 5 shows the reconstruction of temperature and heat flux profile at $t = 5$ s, when the plasma parameters are in steady state, using 2D temperature response function. Such results are obtained by fitting response function to all 143 temperature data on $x$ direction. The temperature response function in equation (2) includes Fourier series with the series number denoted by $n_{max}$ . In figure 5, the fitting is obtained with $n_{max}$ =20. In the top graph, the magenta line and green line correspond to the temperature profile monitored by IR camera and that reproduced by temperature response function, respectively. Although the monitored and reproduced profiles differed at some position, the spatial tendency in temperature profile can be well described using 2D temperature response function. The reconstructed heat flux includes one broad peak at 0 to 60 mm and a very sharp peak at 80 mm. The negative heat flux at x ∼85 mm is a numerical error relating to Fourier series. Such an error is not related to the negative heat flux obtained in figure 5(b).

IR cameras can provide temperature profiles with fine spatial resolution. However, with the technical requirement in future DEMOs as discussed in the previous section, the measurement with IR cameras might be inapplicable. Among several solutions for heat flux analyzing, divertor tile with embedded TCs can be promising. However, the spatial resolution of this method depends on the finite number of TCs so the monitored temperature pattern can not have the good resolution as obtained by IR cameras. The array of TCs needs to satisfy two main requirements. Firstly, the temperature profile must be reasonably reproduced. Secondly, the number of TC must be as few as possible.

To study the impacts of monitoring spacial resolution on the reproduction of temperature profiles, we artificially downsample the temperature profiles into sparse temperature data to emulate TC signals and try to reconstruct them using the 2D response function. The spatial resolution of the sparse temperature profile is denoted by d$x$ and $n_{TC}$ stands for the number of temperature monitoring channels. The temperature profiles in figure 2 have d$x = 1$ mm and $n_{TC} = 143$. To be economical for TC measurements, temperature profiles must be reasonably reconstructed from small $n_{TC}$.

Figure 6 shows the reconstruction of the temperature profile at $t = 5s$ with decreasing the number of $n_{TC}$. Sparse temperature profiles are denoted by green scatters. The blue solid lines are reconstructed by applying the 2D temperature response function to the sparse temperature data. The magenta line corresponds to the temperature profile obtained by IR cameras. With d$x = 7$mm, the broad peak in the area from 0 to 70mm can be well described. The sharp peak at 80mm is underesti-

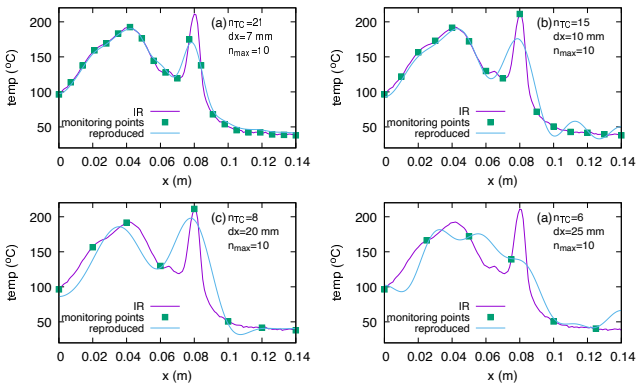


FIG. 6. Effects of $n_{TC}$ =(a) 21, (b) 15, (c) 8, and (d) 6 are investigated to find the fewest monitoring channels that can reasonably reconstruct the temperature profile at t=5s

mated while its width is quite close to that of the IR temperature profile. When d$x$ is reduced to 10 mm, reconstruction in the broad peak remains reasonable. However, uncertainties can be seen at the sharp peak. With d$x = 20$ mm and d$x = 25$ mm, the difference between the monitored profiles and the reconstruction becomes larger. In case of d$x = 25$ mm, the two peak of temperature cannot be recognized.

The monitoring resolution does not need to be so fine to reproduce the broad peak while the sharp peak demands a much higher resolution. $n_{TC}$ dominates the accuracy of reconstruction. Besides, the monitoring position plays an important role. If the field line to the divertor target can be traced in advance, arranging more TCs in the field line area can optimize the number of monitoring positions.

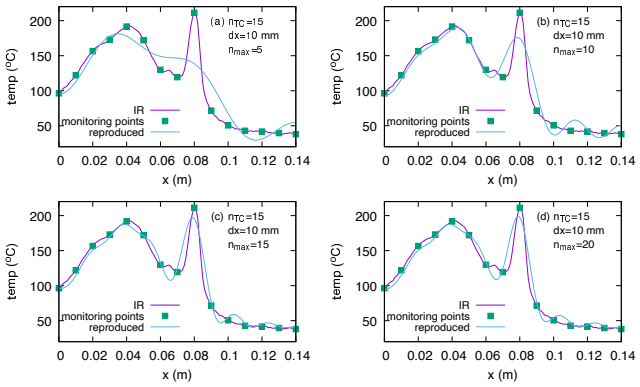


FIG. 7. Effect of fitting series number $n_{max}$ to temperature profile reconstruction at t = 5 s with (a) $n_{max}$=5, (b) $n_{max}$=10, (c) $n_{max}$=15, and (d) $n_{max}$=20.

The temperature response function in equation (2) is composed of Fourier series. If the number of series, denoted by $n_{max}$, is too small, the temperature profile cannot be reproduced precisely. However, if $n_{max}$ is too big, it will cause unnecessary noise fluctuation since the temperature profile is reconstructed with much more functions than the actual monitored data it has.

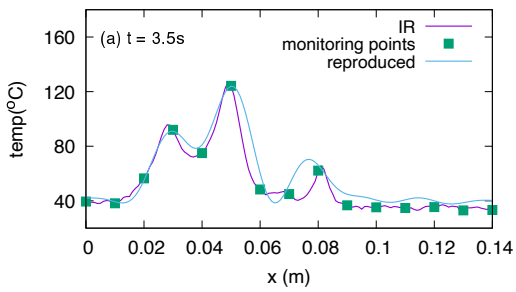


FIG. 8. Temperature profile reconstruction with $n_{TC}$=15, $n_{max}$=15 at (a) t=3.5 s, and (b) t=3.6 s.

Figure 7 shows profiles reconstruction with d$x$ = 10 mm and $n_{TC}$ = 15 with different $n_{max}$ numbers. $n_{max}$ =5 is not sufficient to reconstruct the profile, the two peaks cannot be recognized. With $n_{max}$ = 10, the shape of the broad peak is ensured while the sharp peak is underestimated. When $n_{max}$ increases to 15, both peaks can be reasonably reconstructed and the fluctuation from 100 to 140 mm is reduced. No big differences can be observed when $n_{max}$ increases to 20. It means $n_{max}$ = 15 can be an optimal value to reconstruct this profile.

Figure 8 reveals the reconstruction of temperature profiles at t = 3.5 s. Although this profile is different from the one at t = 5s, it can be reasonably reconstructed with the optimal number of $n_{TC}$ = 15, dx = 10, and $n_{max}$ =15.

### B. Reconstruction of heat flux evolution

The response function is equation (2) is an asymptotic solution which is able to reconstruct the temperature profile. However, to estimate the heat flux evolution, transit solution must be used. By writing the asymptotic solution in equation (2) as $S_{asym}(x,z,t)$, the response function $S(x,z,t) = T(x,z,t) - T_0$ with the transit solution referenced from [15] is described as

$$S(x,z,t) = S_{asym}(x,z) + \Delta T A \sum_{n=0}^{\infty}\sum_{m=0}^{\infty} A_{n,m}\cos(B_n\frac{x}{L_x})\cos(D_m\frac{z}{L_z})\exp(-\tau_{n,m}\frac{t}{\tau}) \quad (4)$$

where $\tau_{n,m} = \frac{4}{\pi^2}((\frac{L_z}{L_x})^2 B_n^2 + D_m^2)$ is defined to satisfy the heat conduction equation. $B_n$ is the same as that for $S_{asym}(x,z,t)$. $D_m = \frac{\pi(2m+1)}{2}$ is determined from boundary condition at $z = L_z$. $AA_{n,m}$ in determined from initial condition when $t = 0$.

Figure 9 reveals the heat flux evolution obtained by pulse decomposition method[16]. This calculation is performed by fitting the temperature response function in equation (4) with the monitored temperature data. At x=80mm, heat flux estimated by the 2D model does not show severe negative values at t=5.5 as observed in the estimation using 1D temperature response function. At x=40mm, however, the heat flux is not terminated after the end of discharge. In our estimation, the target backside is assumed to be perfect heat sink. Such finite values of heat flux after discharge termination in this area mean that the heat is not removed completely from target backside. Besides, there are possibilities that the heat transfers from y-direction. In addition, heat flux profile in our estimation is assumed to be constant during the discharge. So, changes of profile during discharge time might also contribute to such an unreasonable heat flux evolution.

## IV. DISCUSSION AND CONCLUSION

1D temperature response function $S(z,t)$ and pulse decomposition method have been applied to deduce heat flux evolution in several experiments. In the divertor tiles, where the effect of heat flux profile is unavoidable, the 1D estimation model might involve to underestimation of the peak heat flux. Thus, expanding the temperature response function to $x$ direction is necessary. In the present work, we successfully determined 2D temperature response function $S(x,z,t)$ and applied it to LHD divertor tile temperature data at $z = 0$.

The temperature profiles can be reconstructed even with reduced numbers of data points in $x$ direction. With the heat flux profile in the order of cm in LHD divertor tile, we found that 10 virtual thermometer channels would be sufficient to reproduce the temperature profile along the width of 10 cm. This number can even be optimized if magnetic field data is known in advance so that TCs can be concentrated only in the area of consideration. In the future fusion reactor, the sharpness of heat flux profiles depends on magnetic field configurations. Thus, the thermometer channels number must be determined basing on magnetic field data. Temperature signal from TC measurement might be slower when setting TCs further from irradiation surface. Thus, the delay effect must be considered to reproduce temperature evolutions.

If the profile is kept constant during the discharge, it is possible to use the function S(x, z, t ) to obtain the temperature profile evolution from the amplitude of decomposed step heat flux pulse and temperature evolution referenced at only one position (e.g. at x = 40 mm). Besides, the dependence on the heat flux profile can be referenced at only one time slice (e.g. at t = 5 s). In comparison with the temperature data in figure 2, however, the reconstruction does not completely reproduce observed irradiation surface temperature evolution. It means there are changes in the temperature profile during the discharge. To overcome this problem, the profile coefficients must be repeatedly determined to calculate decomposed heat flux size. In addition, improvements relating to the back-side boundary and heat transfer in the third dimension are required

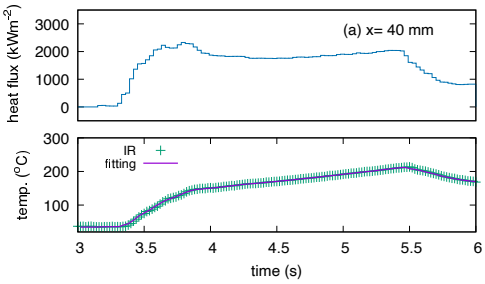


(a) x=40mm

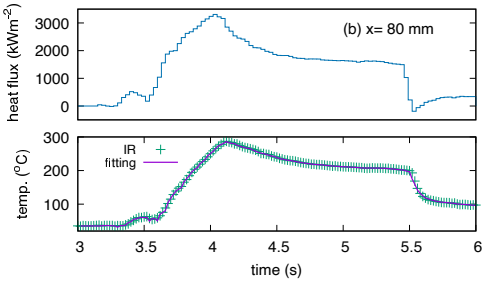


(b) x=80mm

FIG. 9. Heat flux evolutions estimated by pulse decomposition method[16] and $S(x,z,t)$ function at (a) x= 40 mm, and (b) x=80 mm.

to precisely reflect the experiment condition. This will be left for future work.

## ACKNOWLEDGMENTS

The authors wish to thank the LHD experiment group for the excellent support of this work. This work is partially performed with the support and under the auspices of the NIFS Collaborative Research Program (NIFS22KIPR007/ NIFS22KUGM171/ NIFS22KUHL107)

## DATA AVAILABILITY STATEMENT

The data supporting the findings of this study are available in the LHD experiment data repository at https://doi.org/10.57451/lhd.analyzed-data.

[1]A. Loarte, B. Lipschultz, and A. Kukushkin, "Power and particle control [progress in the iter physics basis (pipb)]," *Nuclear Fusion*, vol. 47, 2007.
[2]P. a. Jacquet, L. Colas, M.-L. Mayoral, G. Arnoux, V. Bobkov, M. Brix, P. Coad, A. Czarnecka, D. Dodt, F. Durodie, *et al.*, "Heat loads on jet plasma facing components from icrf and lh wave absorption in the sol," *Nuclear Fusion*, vol. 51, no. 10, p. 103018, 2011.
[3]C. Kang, H. Lee, S. Oh, S. Lee, H. Wi, Y. Kim, and H. Kim, "Study on the heat flux reconstruction with the infrared thermography for the divertor target plates in the kstar tokamak," *Review of Scientific Instruments*, vol. 87, no. 8, p. 083508, 2016.
[4]Y. Hayashi, M. Kobayashi, K. Mukai, S. Masuzaki, T. Murase, L. E. Group, *et al.*, "Divertor heat load distribution measurements with infrared thermography in the lhd helical divertor," *Fusion Engineering and Design*, vol. 165, p. 112235, 2021.
[5]K. Mukai, T. Nishitani, K. Ogawa, and B. J. Peterson, "Neutron shielding design of infrared imaging video bolometer for lhd deuterium experiment," *IEEE Transactions on Plasma Science*, vol. 47, no. 1, pp. 18–21, 2018.
[6]A. Donné, A. Costley, and A. Morris, "Diagnostics for plasma control on demo: challenges of implementation," *Nuclear Fusion*, vol. 52, no. 7, p. 074015, 2012.
[7]K. Tobita, S. Nishio, M. Enoeda, M. Sato, T. Isono, S. Sakurai, H. Nakamura, S. Sato, S. Suzuki, M. Ando, *et al.*, "Design study of fusion demo plant at jaeri," *Fusion Engineering and Design*, vol. 81, no. 8-14, pp. 1151–1158, 2006.
[8]W. Biel, R. Albanese, R. Ambrosino, M. Ariola, M. Berkel, I. Bolshakova, K. Brunner, R. Cavazzana, M. Cecconello, S. Conroy, *et al.*, "Diagnostics for plasma control–from iter to demo," *Fusion engineering and design*, vol. 146, pp. 465–472, 2019.
[9]S. Masuzaki, N. Ohno, and S. Takamura, "Experimental study on plasma heat flow to plasma-facing materials," *Journal of nuclear materials*, vol. 223, no. 3, pp. 286–293, 1995.
[10]S. Takamura, T. Miyamoto, and N. Ohno, "Power transmission factor for tungsten target w/wo fiber-form nanostructure in he plasmas with hot electron component using compact plasma device ait-pid," *Fusion Science and Technology*, vol. 63, no. 1T, pp. 225–228, 2013.
[11]Y. Corre, G. Laffont, C. Pocheau, R. Cotillard, J. Gaspar, N. Roussel, M. Firdaouss, J.-L. Gardarein, D. Guilhem, and M. Missirlian, "Integration of fiber bragg grating temperature sensors in plasma facing components of the west tokamak," *Review of Scientific Instruments*, vol. 89, no. 6, p. 063508, 2018.
[12]J. Gaspar, Y. Corre, M. Firdaouss, J. Gardarein, J. Gerardin, J. Gunn, M. Houry, G. Laffont, T. Loarer, M. Missirlian, *et al.*, "First heat flux estimation in the lower divertor of west with embedded thermal measurements," *Fusion Engineering and Design*, vol. 146, pp. 757–760, 2019.
[13]M. Osakabe, Y. Takeiri, T. Takanashi, K. Tsumori, S. Okamura, K. Matsuoka, R. Akiyama, E. Asano, O. Kaneko, Y. Kawamoto, *et al.*, "Development of fast response calorimeter for neutral beam shine-through measurement on chs," *Review of Scientific Instruments*, vol. 72, no. 1, pp. 586–589, 2001.
[14]J. Ren, D. Donovan, J. Watkins, H. Wang, D. Rudakov, C. Murphy, A. McLean, C. Lasnier, E. Unterberg, D. Thomas, *et al.*, "The surface eroding thermocouple for fast heat flux measurement in diii-d," *Review of Scientific Instruments*, vol. 89, no. 10, p. 10J122, 2018.
[15]H. Matsuura, H. Takeda, K. Ichimura, K. Hosoi, Y. Nakashima, M. Sakamoto, T. Imai, M. Shoji, and K. Nagaoka, "Measurement of divertor heat flux at the end-cell of gamma 10," *Fusion Science and Technology*, vol. 63, no. 1T, pp. 180–183, 2013.
[16]H. Matsuura, K. Nagaoka, T. Morisaki, S. Masuzaki, M. Osakabe, and H. Tanaka, "A new deduction method of heat flux evolution from thermal probe data," *Contributions to Plasma Physics*, vol. 54, no. 3, pp. 285–290, 2014.
[17]H. Matsuura, M. Oouti, M. S. Islam, T. Iijima, R. Minami, and Y. Nakashima, "Comparison of two inverse heat conduction models for heat flux measurement in the gamma 10/pdx," *IEEE Transactions on Plasma Science*, vol. 47, no. 6, pp. 3026–3030, 2019.